Nonadiabatic Coupling in Trajectory Surface Hopping

Isabella Merritt, Denis Jacquemin, Morgane Vacher

Non-adiabatic Coupling in Trajectory Surface Hopping: How Approximations Impact Excited-State Reaction Dynamics

Isabella C. D. Merritt, Denis Jacquemin, and Morgane Vacher*

Nantes Université, CNRS, CEISAM UMR 6230, F-44000 Nantes, France

E-mail: morgane.vacher@univ-nantes.fr

Abstract

Photochemical reactions are widely modeled using the popular trajectory surface hopping (TSH) method, an affordable mixed quantum-classical approximation to the full quantum dynamics of the system. TSH is able to account for non-adiabatic effects using an ensemble of trajectories, which are propagated on a single potential energy surface at a time and which can hop from one electronic state to another. The occurrences and locations of these hops are typically determined using the non-adiabatic coupling between electronic states, which can be assessed in a number of ways. In this work, we benchmark the impact of some approximations to the coupling term on the TSH dynamics for several typical isomerization and ring-opening reactions. We have identified that two of the schemes tested, the popular local diabatization scheme and a scheme based on biorthonormal wavefunction overlap implemented in the OpenMOLCAS code as part of this work, reproduce at a much reduced cost the dynamics obtained using the explicitly calculated non-adiabatic coupling vectors. The other two schemes tested can give different results, in some cases even entirely incorrect dynamics. Of these two, the scheme based on configuration interaction vectors gives unpredictable failures, while the other scheme based on the Baeck-An approximation systematically overestimates hopping to the ground state as compared to the reference approaches.

1. INTRODUCTION

Photochemically active compounds, molecules which react due to exposure to light, are ubiquitous in both nature and human activities forming the basis of photosynthesis,[1] and having applications in fields ranging from medicine to materials.[2–10] Interest in these types of molecules, while always present, has exploded in recent years with the development of sustainable energy sources.[11–13] The synthesis of chemicals in a "green manner" using solar energy via photochemical reactions is also a very active research domain.[14–16] Probing photoreactivity with experimental methods however remains difficult, due to the short-lived character of excited states. In this context first principle calculations are often used to understand photochemical transformations. In particular, the simulation of photochemical reaction dynamics is greatly useful, allowing for the understanding of fundamental mechanisms behind light-driven processes and enabling the design of improved molecules for target applications.

The majority of photochemical reactions are ultrafast and non-adiabatic in nature, i.e., they involve radiationless decay between different electronic states. This decay typically occurs in the vicinity of degenerate points between electronic states of the same spin multiplicity, known as conical intersections (CoIns).[17,18] Modeling non-adiabatic photochemical reactions is challenging, as the Born-Oppenheimer approximation breaks down at and around CoIns, and the coupling between electron and nuclear motion cannot be ignored.[19,20] In such situations, many widely-used and affordable quantum chemistry methods can no longer be relied upon to give accurate results.

Different levels of approximations can be employed when simulating non-adiabatic dynamics, depending on the system size, the desired accuracy, and the level of quantum effects required to describe the process. Towards the more approximate end of non-adiabatic dynamics methods is trajectory surface hopping (TSH).[19,21] It is a mixed quantum-classical method in which the nuclei are treated as classical particles while the electrons are treated quantum mechanically. TSH is built on the idea that an ensemble of independent classical trajectories can be used to approximate fully-quantum wavepacket dynamics through a branching region.[20] Each independent trajectory evolves on a single electronic potential energy surface, with the ability to "hop" from one surface to another.

TSH, more specifically the Tully fewest switches surface hopping (FSSH) variant sometimes referred to in literature as Tully surface hopping, now occupies a privileged spot 30 years after its original description.[21] Indeed it is possibly the most popular non-adiabatic dynamics method, having been applied to model a wide range of photochemical processes.[22–24] Since TSH trajectories are fully non-interacting, they can be run in parallel saving a large amount of computational effort. The on-the-fly nature of the dynamics also means costly electronic structure calculations are only run for sections of the reaction space actually accessed during the dynamics.[20]

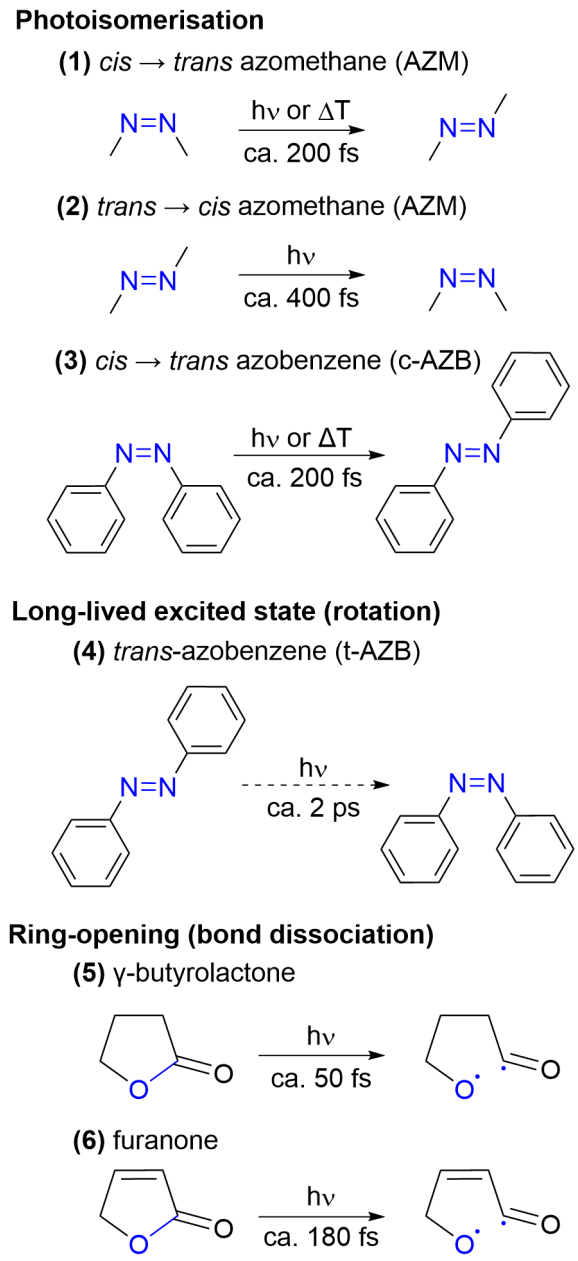

Figure 1: Systems and reactions studied in this work.

While TSH is conceptually a simple method to grasp, there exist, across a number of different quantum chemistry codes, many different TSH schemes known in literature under the same name.[19,25–31] Many of these take advantage of different approximations, in order to run the dynamics on systems of varying size with various electronic structure methods. In particular, different approximations to the non-adiabatic coupling between nuclear and electronic motion are often seen in the literature. These approximations could significantly impact TSH dynamics, since the coupling usually guides if and when classical trajectories "hop" from one state to another - as outlined in more detail in Section 2. In order to assess this effect, five TSH schemes have been identified based on different commonly used approximations for the coupling terms. Their effect on dynamics is investigated considering several model photochemical reactions, given in Figure 1, selected to cover a range of chemical situations.

Reactions **(1)** and **(2)** are respectively the *cis*-to-*trans* and *trans*-to-*cis* isomerization of azomethane (AZM), two simple rotational isomerizations which according to prior simulations take place on different timescales (200 and 400 fs respectively).[23,32] The final photoisomerization reaction, **(3)**, is that of a larger system based around the same central N=N core, *cis*-azobenzene (*cis*-AZB). This molecule isomerizes on a timescale of around 200 fs,[33,34] and is used as a representative of fast photoisomerization in a large system. In contrast, the alternative *trans* isomer (*trans*-AZB) is used as a representative of a "stable" excited state. While this molecule does isomerize upon photoexcitation, the timescale, after S_1 excitation, is on the order of ps (2-16 ps from experiment).[33–35] Thus on the 100 fs simulation timescale, only the initial motions after excitation should be observed. Finally, reactions **(5)** and **(6)** are examples of a different family of reactions, bond dissociations: both describe rapid ring-opening after S_2 excitation. Reaction **(5)** concerns the butyrolactone molecule, which undergoes a ballistic bond-dissociation within 50 fs, while reaction **(6)** concerns the furanone molecule for which the bond-dissociation is slower, *ca.* 180 fs, due to competition with ring-puckering.[36]

As part of this work we have also implemented a new way to perform TSH within the OpenMOLCAS code.[37] It is shown to provide accurate results for the tested reactions while avoiding the expensive calculation of non-adiabatic coupling vectors, thus reducing the cost of TSH simulations in comparison to TSH with the most accurate couplings. We have also implemented a new interface between the Newton-X dynamics package[38] and the OpenMOLCAS code[37] for electronic structure calculations.

2. TSH - A THEORETICAL BACKGROUND

2.1 General theory

In order to best understand the differences between TSH schemes compared herein, we first describe the general theory behind TSH. We then proceed to outline the approximations investigated here and their key differences.

The first approximation made under TSH, fundamental to all implementations of the method, is that the atomic motion can be described by a classical trajectory $R(t)$ - the "classical" part of "mixed quantum-classical" dynamics. Using this idea, an *ansatz* for the time-dependent electronic wavefunction $\Phi(r,t;R(t))$ at time t can be defined in terms of electronic basis functions $\phi_k(r;R(t))$:

$$\Phi(r,t;R(t)) = \sum_k C_k(t)\phi_k(r;R(t)). \quad (1)$$

$\phi_k(r;R(t))$ are often chosen to be the adiabatic solutions to the time-independent electronic Schrödinger equation at geometry $R(t)$. The latter depends on t as defined by the evolution of the trajectory. The expansion coefficients $C_k(t)$ are complex valued, and their norm squared can be interpreted as the "quantum probabilities" for each state in the electronic basis. Essentially TSH can be conceptualized as a classical trajectory evolving according to the gradient of a single electronic state, with an associated electronic wavefunction consisting of all the electronic states weighted accordingly to

their time-dependent coefficients $C_k(t)$.

By substituting the ansatz (1) into the time-dependent electronic Schrödinger equation (2),

$$i\hbar\frac{\partial\Phi}{\partial t} = \hat{H}^{\mathrm{el}}\Phi(t), \tag{2}$$

and carrying out some manipulations (see the SI, Section S1), one obtains the equations of motion (EOM, universal for any TSH implementation) for the expansion coefficients C_k in any orthogonal basis;

$$i\hbar\frac{\partial C_i}{\partial t} = \sum_k C_k\left(H^{\mathrm{el}}_{ik} - i\hbar\left\langle\phi_i\left|\frac{\partial\phi_k}{\partial t}\right.\right\rangle\right). \tag{3}$$

The definition $\left\langle\phi_i\left|\hat{H}^{\mathrm{el}}\right|\phi_k\right\rangle = H^{\mathrm{el}}_{ik}$ is used, with $\hat{H}^{\mathrm{el}}$ being the non-relativistic electronic Hamiltonian operator. In order to get the coefficient for each state at time $t = t + \delta t$, this equation for $\partial C_i/\partial t$ is integrated over the time δt.

The adiabatic states are often used as basis functions in TSH. Since H^{el}_{ik} is diagonal in this basis, the transfer of "quantum probability" between two different states i and k is described solely by the $\left\langle\phi_i\left|\frac{\partial\phi_k}{\partial t}\right.\right\rangle$ term, that is the time-derivative non-adiabatic coupling (TDC) σ_{ik} between these states. When a different basis is used, the off-diagonal terms of H^{el}_{ik} are non-zero and also contribute.

Using the chain rule, the TDC can be expressed exactly as the component of the time-independent non-adiabatic coupling vector (NACV) $d_{ik}(R) = \left\langle\phi_i\left|\frac{\partial\phi_k}{\partial R}\right.\right\rangle$ along the velocity vector of the trajectory:

$$\sigma_{ik} = \left\langle\phi_i\left|\frac{\partial\phi_k}{\partial t}\right.\right\rangle = \frac{\partial R}{\partial t}\cdot\left\langle\phi_i\left|\frac{\partial\phi_k}{\partial R}\right.\right\rangle = \frac{\partial R}{\partial t}\cdot d_{ik}(R). \tag{4}$$

Here we note that this transformation is exact. Should the TDC and NACV be calculated exactly, one would expect TSH results to be identical using either side of Eq. (4) inside Eq. (3) to propagate the coefficients C_k. We note here that both the TDC and the NACV are forms of non-adiabatic coupling between electronic states, with the TDC being the time-derivative analogue of the time-independent NACVs.

The **NACV** TSH scheme used in this work uses this transformation of the TDC to the NACV along the velocity vector. At each timestep the NACVs between all states are calculated and used to propagate the coefficients C_k according to:

$$i\hbar\frac{\partial C_i}{\partial t} = \sum_k C_k\left(H^{\mathrm{el}}_{ik} - i\hbar\frac{\partial R}{\partial t}\cdot d_{ik}(R)\right). \tag{5}$$

To ensure stability of the numerical integration procedures, particularly in cases where the NACV change rapidly between timesteps, the timestep in most TSH implementations is split into smaller "substeps" which are used for numerical integration. A linear interpolation of the energies and NACVs between times t and $t + \Delta t$ is used to obtain the required values for H^{el}_{ik} and d_{ik} at each substep. The only approximations using **NACV** should be those inherent to the TSH theory outlined above, along with any approximations made in the process of integrating the electronic wavefunction. We assume that approximations inherent to integration are equivalent across the schemes investigated and will not detail numerical integration procedures.

In TSH, the classical trajectories evolve on one single electronic state within the basis, with hops occurring based on the chosen switching criterion, at which point the classical trajectory switches to evolve on the new active electronic state. There are multiple ways to compute the hopping probabilities and thus the times when the hops occur along trajectories.[19,39–42] The simplest version assumes that hopping probability is unity if the energy gap between states is smaller than a threshold.[39] More sophisticated algorithms, such as the popular FSSH method, take into account the variation of the wavefunction coefficients and/or the coupling at each timestep.[21,40,41]

In this work, all TSH schemes use the FSSH method[21] to determine the occurrence and location of hops. Under this method, the changes in electronic coefficients are used to determine if a hop occurs, based on a stochastic procedure. FSSH (see the SI, section S1) is designed as a "sensible" set of rules which minimize the number of hops from one state to another while replicating the splitting of a molecular wavepacket by maintaining the correct statistical distribution of trajectories on each state (assuming convergence on number of trajectories). The FSSH algorithm is designed to ensure that the number of trajectories in any state is equal to the average "quantum probabilities" of that state, a property known as internal consistency. In practice the FSSH scheme is usually not fully internally consistent.[43] This is typically the result of two main factors: first, a lack of decoherence within the algorithm itself (usually added through an *ad-hoc* correction),[43,44] and second the presence of "frustrated hops", when the algorithm predicts a hop to a higher state which requires more energy than the nuclear kinetic energy allows.[45,46]

2.2 The Hammes-Schiffer Tully scheme

The Hammes-Schiffer Tully (HST) scheme was originally proposed as an alternative implementation of TSH, using an approximation to the TDC.[26] It is of particular use when the calculation of NACVs is either impossible or prohibitively expensive.[47] HST begins from the formalism of Eq. (3) using the TDCs, and takes advantage of a finite difference method to approximate the TDCs using the overlap between the adiabatic wavefunctions at the start and end of timesteps.

First, the value of the wavefunction ϕ_i at time $t + \frac{\Delta t}{2}$ is approximated as the average of ϕ_i at times $t + \Delta t$ and t:

$$\phi_i\left(t + \frac{\Delta t}{2}\right) \approx \frac{\phi_i(t + \Delta t) + \phi_i(t)}{2}. \tag{6}$$

A finite difference method is then used to approximate the derivative of ϕ_k at time $t + \frac{\Delta t}{2}$:

$$\frac{\partial\phi_k}{\partial t}\left(t + \frac{\Delta t}{2}\right) \approx \frac{\phi_k(t + \Delta t) - \phi_k(t)}{\Delta t}. \tag{7}$$

Using these approximations within the equation for the TDC, and using the orthogonality relation $\langle\phi_i(t)\,|\,\phi_k(t)\rangle = \delta_{ik}$, one arrives at

$$\sigma_{ik}\left(t+\frac{\Delta t}{2}\right) \approx \frac{\langle \phi_i(t) \mid \phi_k(t+\Delta t)\rangle - \langle \phi_i(t+\Delta t) \mid \phi_k(t)\rangle}{2\Delta t}. \tag{8}$$

In other words, the TDC at time $t + \frac{\Delta t}{2}$ can be approximated using the overlap between wavefunctions ϕ_i and ϕ_k at times $t + \Delta t$ and t, where Δt is the timestep used in the surface hopping. Using the same concept the TDC at time $t - \frac{\Delta t}{2}$ can be obtained as:

$$\sigma_{ik}\left(t-\frac{\Delta t}{2}\right) \approx \frac{\langle \phi_i(t-\Delta t) \mid \phi_k(t)\rangle - \langle \phi_i(t) \mid \phi_k(t-\Delta t)\rangle}{2\Delta t}. \tag{9}$$

As the value of σ_{ik} at each substep between t and $t + \Delta t$ is required to carry out the integration of the electronic wavefunction, a straight line between these two points is applied to interpolate for the values of σ_{ik} between times t to $t + \frac{\Delta t}{2}$, and extrapolate for σ_{ik} up to $t + \Delta t$. The HST scheme therefore avoids the need to calculate NACVs or TDC, requiring only the wavefunction overlaps between all states at the start and end of two consecutive timesteps ($t - \Delta t$ and t; t and $t + \Delta t$).

In this work two versions of the HST scheme are included, differing only in the way this wavefunction overlap is obtained, described in detail below. Other ways to obtain the overlap between two wavefunctions can also be found in literature, depending on the electronic structure method employed; e.g., the use of algorithmic screening procedures to select important Slater determinant overlaps between non-orthogonal orbitals at different geometries.[47,48]

2.2.1 HST using scalar product of CI vectors

The first HST based scheme studied here calculates wavefunction overlaps in an approximate fashion, taking the scalar product of the configuration interaction vectors (CIVec). In this case, no further calculation is required to obtain the overlaps, since the CIVecs of the two wavefunctions are available quantities. With this method, one neglects the translation of the orbitals in space, arising from nuclear motion. Any changes in orbital composition and ordering between timesteps are also neglected. This is typically justified by the fact that during a short timestep (on the order of 0.5 fs), both the orbitals and geometry are expected to undergo very limited changes, and so the variation of wavefunctions can be approximated as a change in CIVec-coefficients associated with the same set of orbitals.

This CIVec product based approximation has been implemented as an efficient way to determine state overlaps, not just in dynamics but also to track and follow roots during excited state optimizations.[49] In dynamics, this approximation was used in early works on an alternative non-adiabatic dynamics method, *ab initio multiple spawning* (AIMS),[50] and is key to the vector rotation method successfully employed in QM/MM simulations based on the surface-hopping approach.[51,51,52] In this work, this HST based scheme is referred to as "HST using CIVec product" - **HST(CIV)**: this was the scheme originally implemented in the TSH module in the OpenMOLCAS program.[37]

2.2.2 HST using biorthonormal wavefunction overlap

The second HST based scheme assessed herein calculates the overlap between two wavefunctions by transforming their respective orbitals into a bi-orthonormal basis.[53] Since this scheme is based purely on the orthogonalisation of atom-centered orbitals, it also neglects the translation of the orbitals in space between dynamics steps. However, this is less approximate than **HST(CIV)**, since changes in orbital composition and ordering between timesteps t and $t - \Delta t$ are accounted for.

This scheme is seen to be highly efficient with the complete active space self consistent field (CASSCF) electronic structure method employed in this work. However for some wavefunction based methods such an orbital transformation may significantly enlarge the CI expansion. Thus the efficiency depends on the selected electronic structure level.[48] In this work, we refer to this HST based scheme as "HST using biorthonormalisation" - **HST(BiO)**, which we have implemented as a part of this work in the TSH module in the OpenMOLCAS program.[37]

2.3 The local diabatization scheme

The local diabatization scheme,[25] initially developed in the context of semi-empirical electronic structure methods, represents an alternative approach to both NAC and HST based schemes. Within this scheme, the NACVs/TDC terms are neither calculated nor approximated. Instead, the need for these terms is circumvented by selecting a basis of electronic states in which the TDC is equal to zero - they are "locally" diabatic *along the nuclear trajectory*. Mathematically, this means using a basis η which satisfies,

$$\frac{\partial R}{\partial t} \cdot \left\langle \eta_i \middle| \frac{\partial \eta_k}{\partial R} \right\rangle = \left\langle \eta_i \middle| \frac{\partial}{\partial t} \eta_k \right\rangle = 0. \tag{10}$$

At each timestep, the time-dependent electronic wavefunction, given in Eq. (1) in the adiabatic basis, is transformed and propagated in a locally diabatic basis in which the TDC (between time t and $t + \Delta t$) equals zero. As a result, only the H_{ik}^{el} term in Eq. (3) contributes to the change in diabatic coefficients. At the end of each timestep, the diabatic coefficients are back-transformed to the adiabatic representation.

The diabatic basis is connected to its adiabatic counterpart by the time-dependent unitary transform $U(t)$; $\eta U(t) = \phi$. Expanding the time-dependent electronic wavefunction Φ in terms of the diabatic basis functions one obtains,

$$\Phi(r,t;R) = \sum_k D_k(t)\eta_k(r;R), \tag{11}$$

where the diabatic expansion coefficients D_k are related to the adiabatic coefficients by the same unitary transform matrix $D = U(t)C$. As detailed in the SI (Section S2), the H_{ik}^{el} terms required to propagate D_k can be obtained using the matrix $U(t)$ and the adiabatic energy matrix:

$$H = U(t)E(t)U(t)^{\dagger}. \tag{12}$$

This matrix H is evaluated using Eq. (12) at the end of each timestep. If substeps are used, a linear interpolation is used to obtain H at each substep in order to integrate the electronic wavefunction and thus propagate the electronic coefficients.

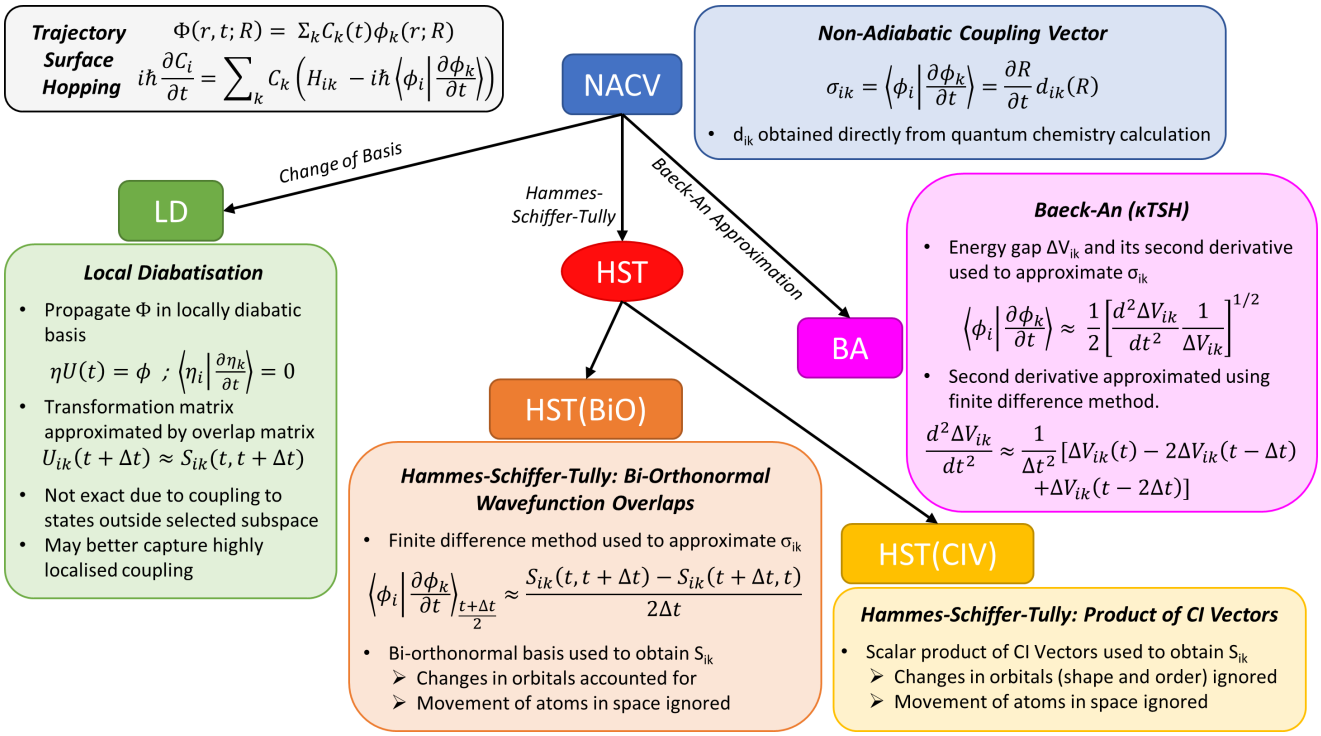

Figure 2: Summary of schemes evaluated in this work and their particular approximations.

Without substeps, the evaluated $H(t+\Delta t)$ is used directly for the integration.

At the beginning of each timestep, the diabatic and adiabatic bases are chosen to be identical at time t, so the transformation matrix is equal to the identity matrix ($U(t) = I$). The diabatic states then differ from the adiabatic states over the time Δt so as to comply with Eq. (10). Thus, to both propagate the electronic coefficients in the diabatic basis, and back-convert to the adiabatic basis, the transformation matrix at the end of the timestep $U(t+\Delta t)$ is the only required new quantity.

It can be demonstrated (SI, Section S2) that, provided there is minimal coupling to states outside of the chosen subspace, $U(t+\Delta t)$ is approximately equal to the overlap matrix between the adiabatic wavefunctions at times t and $t+\Delta t$;

$$S_{ik} = \langle\phi_i(t)\,|\,\phi_k(t+\Delta t)\rangle \approx U_{ik}(t+\Delta t), \qquad (13)$$

This equation is exact in the limit of zero coupling to states outside of the subspace. The overlap matrix used here is calculated using transformation to a bi-orthonormal basis,[53] as in **HST(BiO)**, and thus also neglects the impact of atom translation between timesteps on the orbital overlap. In contrast to the fourfold-diabatization scheme,[54–56] which has also been proposed for use in non-adiabatic dynamics with multi-reference wavefunctions, the local diabatization does not change the molecular orbitals and is path-dependent. We refer to this TSH scheme, using a diabatic basis, as the local diabatization scheme: **LD**.

2.4 The Baeck-An Scheme

Recently, Baeck and An proposed that the NACV (in 2D) between two states near to a CoIn can be approximated using only the energy gap and the second derivative of this energy difference with respect to the coupling direction.[57] This approximation has recently been extended to TSH under different formalisms.[27,29] This approach, sometimes named κTSH,[27] avoids calculation of both NACVs and wavefunction overlaps, making it less computationally expensive and potentially beneficial for dynamics on emerging machine learning potentials where wavefunctions and NACVs may not be available.[58,59]

The Baeck-An approximation can be generalized to approximate the TDC (for $i > k$),

$$\sigma_{ik} = \left\langle\phi_i\middle|\frac{\partial\phi_k}{\partial t}\right\rangle \approx \frac{1}{2}\left[\frac{d^2(V_i - V_k)}{dt^2}\frac{1}{V_i - V_k}\right]^{1/2}, \qquad (14)$$

where V_i is the adiabatic energy of state i. The TDC for $k > i$ can be obtained using $\sigma_{ik} = -\sigma_{ki}$.

The second derivative of the energy gap can be approximated either using the gradients of all states, or simply using the energy gap $\Delta V_{ik} = V_i - V_k$. Since calculating all gradients would add significant cost to TSH simulations, hence removing much of the interest in this approach, the energy gap formalism is used, where

$$\frac{d^2(V_i - V_k)}{dt^2} \approx \frac{1}{\Delta t^2}[\Delta V_{ik}(t) - 2\Delta V_{ik}(t-\Delta t) + \Delta V_{ik}(t-2\Delta t)]. \qquad (15)$$

Higher-order approximations can also be used to obtain this second-derivative of the energy gap.[29]

This scheme is a recent addition to the possible ways to run non-adiabatic dynamics, and as a result it has not yet

seen widespread use (unlike the previously mentioned NAC, HST and LD schemes). Previous tests led to rather conflicting conclusions to its accuracy compared to other TSH schemes.[27,29] We refer here to TSH using the generalized Baeck-An approximation as the Baeck-An scheme, **BA**.

2.5 Summary

Figure 2 provides a visual summary of the associated key features and approximations made within each of the five schemes studied in this work; **NACV**, **LD**, **HST(BiO)**, **HST(CIV)** and **BA**. We note that while these five schemes do not constitute a comprehensive list of all ways to run TSH available and described in the literature, we trust that they cover a wide range of possible TSH schemes. In particular, we have focused on schemes which are the default within codes which are popular and regularly used within the field of surface-hopping dynamics, by both expert and non-expert users.

3. COMPUTATIONAL DETAILS

3.1 Electronic Structure

All electronic structure calculations are carried out using the OpenMOLCAS program.[37] For all molecules studied, state-average complete active space self consistent field (SA-CASSCF) calculations are used to describe the electronic structures.[60] Active spaces and state average number selected for each molecule are:

- AZM - 2SA-CASSCF(6e,4o)
- AZB - 4SA-CASSCF(14e,12o) and (6e,4o)
- Butyrolactone - 3SA-CASSCF(10e,8o)
- Furanone - 3SA-CASSCF(12e,10o)

The full orbital descriptions of each are given in the SI, Section S3.

For both AZB, butyrolactone and furanone, the relativistic core-correlated atomic-natural orbital basis set with polarized double-ζ contraction ANO-RCC-VDZP is used.[61] For AZM the 6-31G(d) basis set[62] with a single set of *3d* polarization functions[63] on the C and N centers is used to allow comparison to previous literature.[23] Resolution-of-identity based on the Cholesky decomposition is used throughout to speed up electronic structure calculations.[64]

3.2 Dynamics simulations

Initial conditions for dynamics are generated with Newton-X,[38] sampling geometries and velocities (in an uncorrelated fashion) from the Wigner distribution (without temperature broadening) using harmonic frequencies calculated at the respective electronic structure level at the relevant optimized ground state geometry for each reaction. Initial conditions for 100 trajectories are sampled for all studied reactions, except *trans*-AZM and butyrolactone which both require 200 trajectories for convergence of the results. Proof of convergence on number of trajectories for all reactions can be found in the SI (section S4).

Several programs are used to run the *ab initio* surface-hopping mixed quantum-classical dynamics. **NACV** and **LD** simulations are carried out using two different codes interfaced to OpenMOLCAS:[37] SHARC[65–67] and Newton-X,[38,68] the OpenMOLCAS interface for the latter has been written as part of this work.[37] **HST(BiO)** and **HST(CIV)** simulations are carried out using OpenMOLCAS for both dynamics and electronic structure.[64] **HST(BiO)** has been implemented in the currently available repository of OpenMOLCAS as a part of this work. **BA** simulations are carried out using the SHARC-MN(v1.2) extended version of SHARC.[65,69]

In OpenMOLCAS, a timestep of 20 a.u. (0.48 fs) is chosen for the integration of Newton's equations using the Velocity-Verlet algorithm, with the integration of the electronic wavefunction at each timestep split into 96 substeps. In SHARC, a timestep of 0.5 fs (20.7 a.u.) split into 100 substeps is chosen to ensure nearly equivalent substep timelength. In Newton-X, a timestep of 0.5 fs is also selected; the **LD** scheme however in Newton-X does not include substeps. In all schemes the energy based Persico-Granucci decoherence correction is used, with a decay factor of 0.1.[43] Energy conservation has been checked for all simulations run, checking for active space stability, intruder states, and other simulation artifacts. A maximum of six trajectories per ensemble (for *trans*-AZB) are rejected due to insufficient energy conservation. The location of hops is determined in each scheme by the FSSH algorithm (with original probabilities as given by Granucci *et al.*[25] used for **LD**). For all simulations, total energy is conserved by rescaling the velocity. While rescaling along the NACV component of the velocity has been demonstrated to be the best choice in TSH,[70] this is only possible when NACVs are calculated. In order to compare all schemes fairly, we instead rescale along the velocity vector. This scaling is not expected to strongly impact the dynamics.[71]

We would also like to highlight an important and sometimes overlooked component of TSH simulations: the absolute phases of electronic wavefunctions. The latter are arbitrary in the independent electronic structure calculations performed across the different timesteps. While the absolute signs of the electronic wavefunctions do not affect the electronic state energies and gradients, they directly imprint onto the NAC vectors or wavefunction overlaps. This can thus impact the electronic coefficient propagation and consequently, the possible trajectory "hops". Care for phase consistency along a trajectory must then be taken and we have implemented and/or checked for phase correction in all simulations reported here. We have also compared the results using different phase correction schemes (wavefunction overlap and scalar product of NAC vectors) to ensure this has no effect on the conclusions regarding the various TSH schemes.

4. RESULTS

For all reactions, to compare the results of different TSH schemes the electronic populations are first plotted as a function of time; these are defined as the fraction of trajectories on each active state as discussed in section 2.1. These population evolutions provide convenient overviews of the differences arising from the different approximations to non-adiabatic coupling along the trajectories, since variations in the rate of change of electronic populations between schemes arise from different locations in time of the hops. We then analyze the impact on the actual photoreaction processes, e.g., yields

and rates of product formation.

4.1 Photoisomerization of *cis*-Azomethane

We begin with the prototypical *cis (Z)* to *trans (E)* photoisomerization of AZM. This relatively rapid process occurs after exciting to the first ($n\pi^*$, S_1) excited state, in ca. 200 fs according to previous simulations.[23]

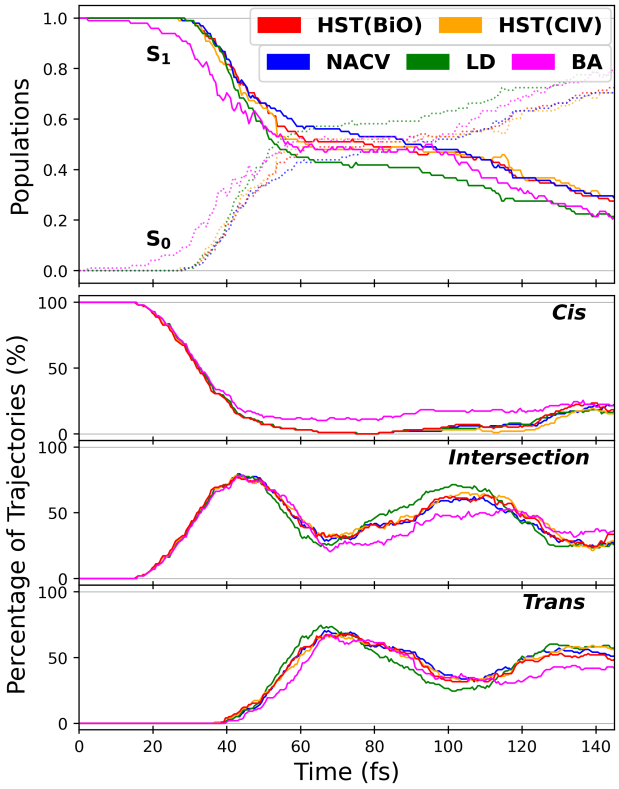

Figure 3: The *cis* → *trans* S_1 photoisomerization of azomethane (reaction **1**): electronic populations and fractions of trajectories assigned to each isomer over the 145 fs simulated.

Figure 3 shows the same qualitative decay profile with all schemes, starting with a rapid decay to ca. 50% S_1 population within 60 fs, followed by a slower decay starting around 100 fs. According to previous theoretical studies,[23] the photoisomerization proceeds through a rapid rotation about the central C-N=N-C moiety, reaching a S_1/S_0 conical intersection (CoIn) roughly halfway between the *cis* and *trans* isomers around t = 40 fs. This is seen in the relative fraction of *intersection* trajectories present throughout the simulations: the first peak of this fraction appears at ca. 40 fs for all schemes. The population changes seen in the initial 60 fs are explained by $S_1 \rightarrow S_0$ decay occurring through this first CoIn.

The C-N=N-C rotation is a fast, energetically favored process, and with the excess energy in the system the molecule rotates past the CoIn located around C-N=N-C = 90° to angles where the decay is no longer likely to occur. This is seen directly in the plot of the isomers, and reflected in the relative plateau in the S_1 decay between 60 and 100 fs. When the rotation has completed another 180° from the first S_1/S_0 CoIn, it reaches another symmetry equivalent CoIn seen clearly around 110 fs in the fraction of *intersection* trajectories, through which the second decay occurs beginning around 100 fs. In previous simulations, trajectories which decay through this second intersection, i.e., after a 270° total rotation, have been referred to as *rotator* trajectories and were associated with different *cis* versus *trans* product yields as compared to the *standard* trajectories.[23]

Table 1: Comparison of *cis*-azomethane dynamics results for different TSH schemes: fraction of trajectories decayed at the end of the simulations (145 fs), final *standard (Std.)*/*rotator (Rot.)*/*other (Oth.)* ratio of trajectories, and isomerization quantum yield $QY_{c\rightarrow t}$ (see text).

Method	Final State		Trajectory Types		$QY_{c\rightarrow t}$
	S_0	S_1	*Std.*	*Rot.*	
NACV	71	29	66.2	33.8	0.55
LD	79	21	74.7	25.3	0.58
HST(BiO)	72	28	70.8	29.1	0.57
HST(CIV)	70	30	76.1	23.9	0.59
BA	79	21	66.7	33.3	0.56

Table 1 compares the percentage of trajectories which have relaxed to the ground state by the end of the 145 fs simulated, along with the fraction of these decayed trajectories labeled as *standard* or *rotator* depending on which CoIn they are closest to when decay occurs (ignoring decays followed by back-hops within 10 fs). The simulations are too short to directly obtain reliable estimates of the photoisomerization quantum yields $QY_{c\rightarrow t}$: the fraction of isomers present is still clearly fluctuating at the end of the simulation, with 25–30% at the intersection. In addition, the lack of a pathway for the molecule to dissipate the energy obtained from excitation implies that the excess vibrational energy should be more than sufficient to cross the small thermal barrier between *cis* and *trans* AZM multiple times after $S_1 \rightarrow S_0$ decay, meaning stable values may be challenging to obtain. However, using the associated product yields for *standard* and *rotator* trajectories from literature simulations[23] the $QY_{c\rightarrow t}$ for each scheme can be estimated, and these are also given in Table 1.

For all schemes except **BA**, the non-adiabatic relaxation starts at almost exactly the same time, ca. 30 fs, while **BA** shows decay beginning at ca. 20 fs. From the location of the hops for each scheme (Figure S7 in the SI), it is clear that hops can occur further from the CoIns using **BA**, and some hops even occur while the molecule is still in the *cis* form. This is also the origin of the differences in the *cis* fraction throughout the simulations: the 12% of trajectories which relax very early in fact never reach the first intersection, and rotate back to reform *cis*. Otherwise, the overall decay from S_1 over the simulations is similar for all schemes. **NACV**, **HST(BiO)** and **HST(CIV)** are most similar, with around 29% remaining in S_1 by 145 fs. In contrast, **LD** and **BA** induce larger overall $S_1 \rightarrow S_0$ decay, with only 21% remaining in S_1 at 145 fs. For **LD**, this difference results from around 10% more decay occurring through the first CoIn, while for **BA** it seems mostly to result from decay occurring further from both CoIns. There is also significantly more back-hopping observed with **BA**: 55% of trajectories undergo at least one back-hop to S_1 after initial decay, compared to 7% only with **NACV**.

The splitting of decayed trajectories into *standard* and *ro-*

tator shows a larger fraction of *standard* trajectories with **LD** and **HST(CIV)** than the other schemes. From the *standard*/*rotator* splitting one sees that **HST(CIV)** differs a similar amount from the **NACV** results as **LD**, a result less visible in the overall decay. As expected, the QY calculated as outlined above follow these splittings, with **HST(BiO)** and **BA** closest to **NACV**, while **LD** and **HST(CIV)** give higher QYs. However, although the splitting between relaxation pathways varies by 10%, the variation in QY is smaller at $\Delta QY_{c\to t} = 0.03$: larger differences in electronic decays here have a rather small influence on the overall reaction dynamics. In general all coupling schemes provide quantitatively similar results for this photoreaction. Yet we underline that even for this simple case some differences in pathway repartitions are seen depending on the selected approximations.

4.2 Photoisomerization of *trans*-Azomethane

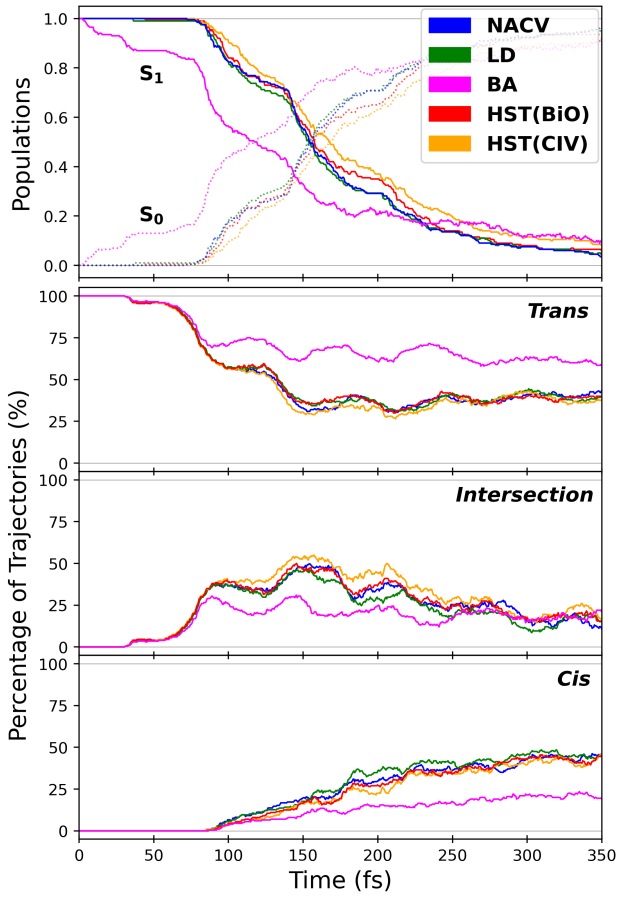

Figure 4: The *trans* → *cis* S_1 photoisomerization of azomethane (reaction **2**); (a) electronic populations and (b) fractions of trajectories assigned to each isomer over the 350 fs simulated.

We now move to investigate the dynamics of the opposite isomerization process, *trans (E)* to *cis (Z)*, which also occurs after exciting to the first excited state. In comparison to the above process, this reaction proceeds on a slower timescale, ca. 400 fs according to prior simulations.[23,32] Indeed, since the S_1 surface in the C-N=N-C rotation coordinate is less steep for the *trans* isomer than the *cis*, a longer time is needed to reach the same S_1/S_0 CoIn around C-N=N-C = 90°.

The decays of the S_1 state for this reaction, seen in Figure 4, follow a relatively standard shape for the decay through a single CoIn for all schemes. The S_1 decay contains two small plateaus around 125 and 180 fs, corresponding to slight dips in the *intersection* trajectory fraction: some groups of trajectories arrive at the S_1/S_0 CoIn earlier than others (see Figure S8 in the SI). All schemes except **BA** give very similar results for both electronic populations and trajectory fractions. Both **HST(CIV)** and **BA** slightly underestimate the overall $S_1 \to S_0$ decay by ca. 5%, and **HST(CIV)** has less distinct plateaus around 125 and 180 fs. **BA** contains these plateaus, but shows a decay of ca. 15% within the first 75 fs, while all other schemes only begin decaying after 75 fs. The overall $S_1 \to S_0$ decay after this point is then around 20% lower than for the other schemes (besides **HST(CIV)**) resulting in a similar final S_1 population to **HST(CIV)**.

Again stable values for the quantum yields cannot be obtained: a fraction of ca. 20% *intersection* trajectories remain after 350 fs, and again we expect the small thermal barrier on the ground state to be easily crossed after the decay thanks to excess vibrational energy. However, the fraction of trajectories classified as *trans* and *cis* throughout the simulations can be compared. All schemes behave almost identically for the first 80 fs, before splitting between **BA** and the other schemes occurs with a much larger fraction of trajectories remaining in *trans* form: around 30% more, resulting in reduced *cis* and *intersection* fractions. Later, around 100 fs, **HST(CIV)** also separates slightly from the other schemes, with slightly more *intersection* trajectories, however, this difference does not persist to the end of the simulations with similar final *trans* and *cis* fractions to the other schemes. In contrast, the difference in **BA** persists throughout, with ca. 20% less *cis* being produced by the end of the simulation. This is expected to result in an underestimation of at least 20% of the photoisomerization QY of *trans*-AZM.

The geometric locations where strong coupling is translated into $S_1 \to S_0$ hops in the five schemes can also be compared: Figure S9 in the SI shows the cumulative fraction of hops which occur as a function of the central C-N=N-C dihedral angle, a crude representation of the rotational reaction coordinate with the minimum energy CoIn being located around 90°. With **HST(CIV)**, the hops are slightly delayed (by 1–2°) along the rotational coordinate compared to **LD**, **NACV**, and **HST(BiO)** indicating that this approximation may lead to a slight underestimation of coupling further from the CoIn. However, this has no noticeable effect on the fractions of trajectories throughout. In contrast, the differences using **BA** are much clearer, with hops seen at all dihedral angles, although more hops are seen nearer to the CoIn around 90°. This is clearly seen in the plots showing the location of hops and the evolution of the CNNC angles (Figure S8 in the SI), and results in a reduced *cis*-AZM yield as hops earlier along the rotation favor reforming the *trans* isomer.

Overall, all schemes aside from **BA** provide quantitatively similar results for the *trans*-to-*cis* photoreaction. From the isomer plots, QY of photoisomerization are expected to be even more similar than the previously discussed *cis*-to-*trans* direction, except for **BA** which is expected to underestimate the QY by ca. 20%.

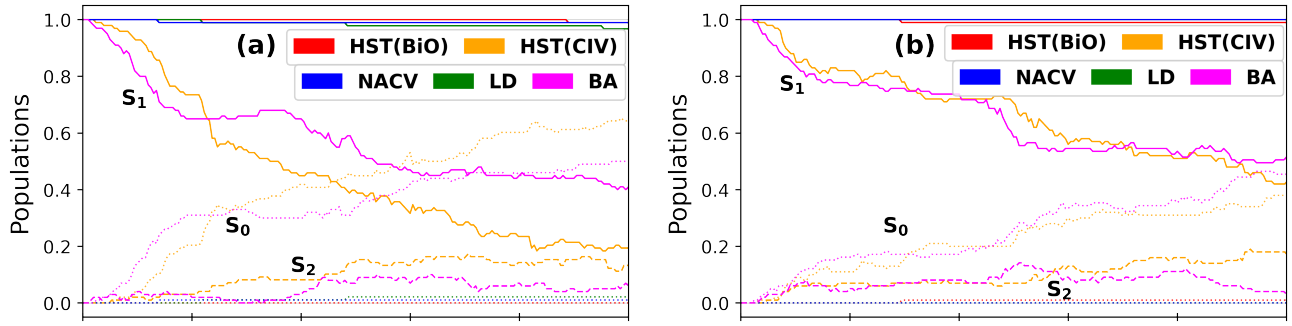

Figure 5: Electronic populations over the 100 fs simulated after the S_1 excitation of *trans*-azobenzene (system **4**) using (a) a "large" (14e, 12o) and (b) a "minimal" (6e, 4o) active space. S_2 populations (dashed line) are shown only for **BA** and **HST(CIV)** for clarity, all other schemes have negligible S_2 populations throughout. S_3 populations are also not shown as these are negligible throughout for all schemes.

4.3 S_1 excitation of *trans*-azobenzene

Next, let us look at a larger compound containing the same photoreactive chromophore, the *trans*-AZB. This system is interesting since, while the excitation to S_1 does induce a rotational isomerization around the central C-N=N-C bond as in AZM, experiment and prior simulations give a 2–16 ps timescale for this reaction.[33–35] Thus on the simulated 100 fs timescale, one can view the system as a "stable" excited state: the coupling between states should remain very small since the system remains far from any CoIn, and few if any hops should occur.

Figure 5(a) shows this expected behavior of approximately constant S_1 population for all schemes except **HST(CIV)** and **BA**. **HST(CIV)** and **BA** yield rapid S_1 decays, reaching 50% within the first 30 fs and 50 fs, respectively. The S_1 population mostly transfers to the S_0 state, but there is some small transfer upwards to the S_2 and S_3 states. As was seen for AZM, in the **BA** simulations the $S_1 \rightarrow S_0$ decay again happens far from any CoIn, the average energy gap at hop locations being 1.63 eV. At such a large separation of states, it is unexpected to see non-adiabatic coupling to such a magnitude which could lead to a decay of 60% of the overall S_1 population within 100 fs. It appears that approximations within the **BA** scheme break down at points far from CoIns. On the other hand, **HST(CIV)** did not show such behavior before for the AZM reactions, suggesting an explanation specific to the larger AZB system is required to describe this unphysical decay. Since **HST(CIV)** gives results inconsistent with experimental observations[33–35] while **HST(BiO)** does not, the problem must arise not from approximations within the HST scheme itself but instead from the additional approximations made in the calculation of the overlap matrix S_{ik}.

In the **HST(CIV)** method, changes in both orbital shape and ordering are ignored - the overlap being calculated as a scalar product of the configuration interaction vectors between two timesteps. This approximation is therefore expected to break down when significant orbital changes occur between timesteps. Analyzing the **HST(CIV)** trajectories hopping from S_1 to S_0 within the first 40 fs, we find discontinuities in the σ_{ij} coupling term calculated using **HST(CIV)** (Figure S12 in the SI), which indicates that the changes in orbitals between timesteps may be not only significant but discontinuous in nature. Upon inspection of their evolutions, we discover that not only do orbitals change thanks to mixing and nuclear displacement, but also that the character of specific orbitals within the CASSCF active space can entirely change from one timestep to the next (Figure S14 in the SI). We note however that these changes and swaps occur within a stable active space, i.e., the potential energy surfaces are continuous.

This problem actually originates from a fundamental principle of CASSCF, that the results are invariant to orbital ordering and rotations within the active space. Mixing and unmixing of orbitals can lead to orbitals of different character "swapping places" within the arbitrary active space ordering. When approximating the overlap term S_{ij} as a scalar product of CI vectors, this possibility is unaccounted for. Since this is not due to actual differences between the CASSCF solutions at two timesteps, and only due to arbitrary ordering within the active space (which could differ between two identical CASSCF solutions), this effect is not avoided by decreasing the timestep (Figure S13 in the SI). If the orbitals change significantly but gradually over time without discontinuities due to orbital reordering, as in the previously described AZM photoisomerizations, **HST(CIV)** can yield coherent results.

In *trans*-AZB however, it appears that the rapid decay in the first 30 fs is related to discontinuities in the coupling term arising from reordering of orbitals in the active space. One can hypothesize that this problem is more likely to be seen with a large active space containing more orbitals which can swap or mix. This hypothesis is tested using the minimal active space required to describe the photochrome, i.e., excluding π/π^* orbitals related to the phenyl rings and selecting the (6e, 4o) active space describing the C-N=N-C chromophore, equivalent to that used for AZM.

Using this minimal active space for *trans*-AZB, a significant improvement of the **HST(CIV)** results is seen in Figure 5(b), with the disappearance of the rapid $S_1 \rightarrow S_0$ decay within the first 30 fs. The evolution of the coupling term over time for this smaller active space (Figure S12 in the SI) is smooth, with no discontinuities. Nevertheless a slower decay with a half-life of ca. 100 fs is still obtained, which can also be seen at later times with the larger active space. This 100 fs decay with **HST(CIV)** arises from additional overestimation of the σ_{ij} term. From hop locations, this decay is associated with a symmetrical opening of the two

C-N=N valence angles. While a C_{2h} CoIn characterized by this motion does exist, it is located much further along this coordinate and should also be inaccessible after S_1 excitation, being significantly higher in energy than the S_1 state at the Frank-Condon geometry. In short, for *trans*-AZB **HST(CIV)** is also overestimating the coupling at points far from a CoIn.

Interestingly, **HST(CIV)** and **BA** give similar results using this minimal active space, suggesting the overestimation of coupling far from CoIns is similar in both schemes. Using the smaller active space leads to a slightly slower decay for **BA** than when using the full (14e, 12o) active space. Changing the active space results in different potential energy surfaces, and in this case excluding the π/π^* orbitals results in the movement along the symmetrical opening of the C-N=N angles being less favorable. Looking at the average potential energies for the **NACV** simulations (Figure S15 in the SI), the energy gap between S_1 and S_0 reduces in the first 20 fs of the simulations before increasing again. Using the full (14e, 12o) active space, the smallest energy gap is 1.1 eV, while in contrast using the minimal (6e 4o) active space the smallest energy gap is larger (1.5 eV). Using the smaller active space appears to make this planar CoIn even less accessible, reducing the decay in these two schemes.

Finally, the fractions of isomers throughout the trajectory (Figure S12 in the SI) have also been investigated, as for the AZM reactions. Almost constant 100% *trans* is seen as expected for all schemes except **HST(CIV)**. The latter results in a small fraction of the trajectories being *intersection* type after 100 fs: ca. 7% for the full (14e, 12o) active space, and ca. 6% for the minimal (6e, 4o) one. Although the minimal active space gives much more physical results for the electronic decay, for the nuclear dynamic process it gives only slightly better results. Additionally, even though the use of a smaller active space can help with failures of **HST(CIV)**, it can also yield unintended harmful effects if important orbitals to describe the system are neglected: a careful selection of active space is obviously critical in any CASSCF calculation. **BA** gives the expected 100% *trans* throughout the simulations, despite its similar $S_1 \rightarrow S_0$ decay similar to **HST(CIV)**. However, using the smaller active space around 6% of the trajectories finish as *intersection type*: an example of reducing active space leading to unintended results.

Since the *trans* to *cis* isomerization reaction of AZB takes place on a much longer timescale, extrapolating the 100 fs simulated to obtain any estimate of final quantum yields after 2–10 ps is impossible. However, the ultrafast $S_1 \rightarrow S_0$ decay seen in both **HST(CIV)** and **BA** while the molecule remains mostly planar is expected to cause a significantly underestimated quantum yield, since the isomerization is known to take place via slow rotation while on the S_1 surface (which would clearly be impossible after ultrafast S_1 deactivation).

4.4 Photoisomerization of *cis*-azobenzene

The logical next step is the S_1 photoisomerization of *cis*-AZB. Unlike its *trans* counterpart, the S_1 state is known to be short lived for *cis*-AZB: both experiment and prior simulations give isomerization in ca. 200 fs.[33,34] This allows investigation of TSH coupling approximations on the photoisomerization of a system larger than AZM.

From Figure 6, we can see that the electronic populations for both **BA** and **HST(CIV)** differ from the other three schemes, which are in good agreement. **HST(CIV)** shows a faster S_1 decay but which starts at the same time as the other three schemes, while **BA** shows a decay of similar rate to the other three schemes but starting immediately, without an initial 20 fs delay. Clearly **HST(CIV)** is again unable to accurately describe the $S_1 \rightarrow S_0$ decay while **HST(BiO)** is successful. We again attribute this to the overlap approximation used, and note that this approximation does not only fail for "long-lived" excited states. The failure is likely related to the active space size and its impact on orbital changes between timesteps. Indeed, when the *cis*-AZB active space is reduced, as in the previous Section, specific inaccuracies of the **HST(CIV)** approximations are reduced and all electronic decays (besides **BA**) become similar (Figure S17 in the SI). **BA** again shows significant decay at very early points in the simulations, before the molecule is expected to reach a region of high non-adiabatic coupling.

Nevertheless, for this fast *cis*-AZB photoisomerization the inaccuracies of **HST(CIV)** are less remarkable than for its *trans*-AZB counterpart, where the breakdown of **HST(CIV)**

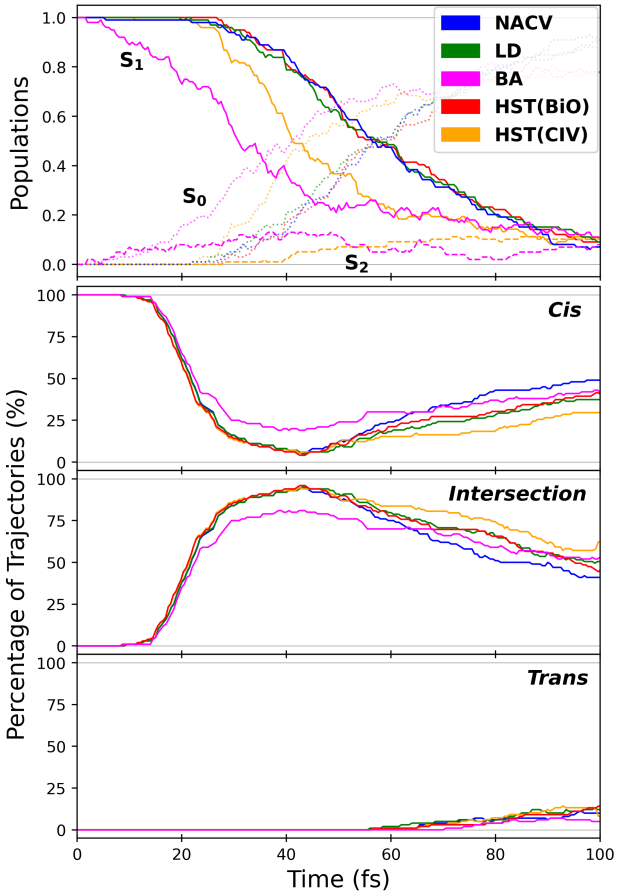

Figure 6: The *cis* → *trans* S_1 photoisomerization of azobenzene (reaction **3**) using a "large" (14e, 12o) active space: (a) electronic populations and (b) fractions of trajectories assigned to each isomer over the 100 fs simulated. S_2 populations (dashed line) are shown only for **BA** and **HST(CIV)** for clarity, all other schemes have negligible S_2 populations throughout. S_3 populations are also not shown as these are negligible throughout for all schemes.

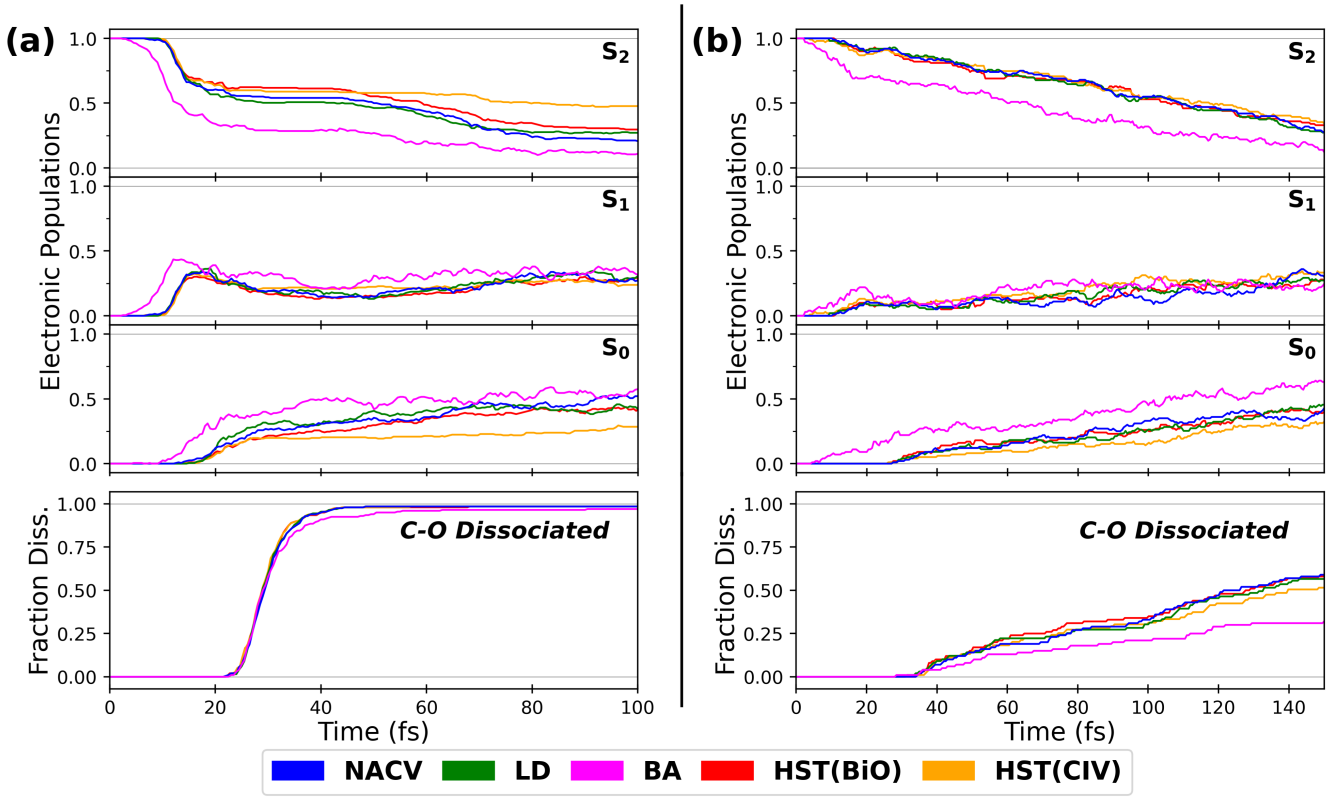

Figure 7: Electronic populations and fractions of dissociated trajectories during the S_2 photoinduced ring-opening of (a) butyrolactone (reaction **5**) and (b) furanone (reaction **6**).

led to relaxation through a CoIn normally inaccessible to the dynamics. In contrast, the hop locations (SI, Figure S18) for the *cis*-AZB reaction indicate that the **HST(CIV)** relaxation proceeds through the same CoIn as the other schemes, at indeed the key intersection previously located in literature.[72,73] The **HST(CIV)** hops begin to occur a few degrees earlier along the central C−N=N−C rotational coordinate, so at a slightly further distance from the CoIn, which could have a minor influence on later-time dynamics. The **BA** hops begin to occur significantly further from the intersection, as early as at 20° twist (while the CoIn is at ca. 90°). However more than 50% of the hops do still occur within 30°of the CoIn.

The fractions of isomers present throughout the simulations are also compared in Figure 6. Again here both **BA** and **HST(CIV)** show the most differences to the other schemes. The main difference in **BA** is that the peak in the *intersection* fraction around 40 fs is lower, this difference being compensated by a larger *cis* fraction at this point. However, these fractions come back in line with the other schemes by around 60 fs, and no major difference is seen after this. The effect of this early reduction of *intersection* trajectories is impossible to predict on the longer time dynamics, but increased hopping at earlier C−N=N−C rotation angles nearer to the *cis* initial isomer could lead to reduced photoisomerization yield. In comparison, differences in **HST(CIV)** are seen after 50 fs, and are only seen in the fractions of *cis* and *intersection* present, reflecting different speeds for the formation of *cis*-AZB from the intersection. **HST(CIV)** is slowest, with around 10% less *cis* formed by the end of the simulations compared to the other three schemes. The impact of this difference on the final quantum yield cannot be easily predicted, although producing *cis* slower but *trans* at the same rate could lead to larger final amounts of *trans*-AZB, i.e., overestimated photoisomerization quantum yields from **HST(CIV)**.

4.5 Photoinduced ring-opening of butyrolactone and furanone

Finally, the performance of the five schemes was tested on a different type of reaction, the bond-dissociation taking place in the photoinduced ring-opening of both butyrolactone and furanone after excitation to the S_2 state. For butyrolactone, this reaction is a very rapid ballistic ring-opening process with the C-O bond predicted by simulations to break within the first 50 fs.[36] In contrast, the equivalent ring-opening process in furanone is predicted to take around 180 fs due to competition with ring-puckering.[36]

We begin by analyzing the electronic population evolutions for butyrolactone, shown in Figure 7(a). All schemes give similar results for electronic populations decays, except for **HST(CIV)** and **BA**. **HST(CIV)** is unable to correctly describe the populations from around 40 fs onward, with S_2 being overestimated and S_0 underestimated. **BA** predicts a larger overall decay from S_2, mostly due to 28% of trajectories decaying from $S_2 \rightarrow S_1$ within the first 10 fs, before any other scheme starts decaying. Aside from this initial decay only seen with **BA**, the S_2 decay can clearly be divided into two distinct regions: a first rapid decay between 10–30 fs, and a second slower decay between 45–90 fs. The values of population losses from S_2 during the two periods of time are

given for each scheme in Table 2.

Table 2: Comparison of butyrolactone dynamics results for different TSH schemes: fraction of trajectories which decay from the S_2 state in the first (10–30 fs) and second (50–90 fs) decay regions, and total S_2 decay over the full 100 fs simulated.

Method	First S_2 decay %	Second S_2 decay %	Total S_2 decay %
NACV	45	31	77
LD	50	22	72
HST(BiO)	38	29	69
HST(CIV)	41	11	52
BA	43	16	88

The failure of **HST(CIV)** to correctly describe the second S_2 decay and thus all populations from 30 fs are again attributed to obtaining the overlap from the CIVec scalar product. This is supported by the **HST(BiO)** results, which are able to correctly reproduce the electronic decays from both **NACV** and **LD**. On the other hand, the differences using **BA** are again due to early decay, with this scheme predicting decay at points far from the CoIn. Other than this initial decay, the first *normal* decay (10–30 fs) is well reproduced by **BA**, while the second S_2 decay is underestimated as in **HST(CIV)**. The latter is likely due to the reduced available S_2 population induced by the earlier first 10 fs decay.

We can turn to Table 2 to break down quantitative differences between the other three schemes. For the first decay **NACV** and **LD** are most similar with **LD** having only 5% higher decay than **NACV**, while **HST(BiO)** underestimates this decay by 7% as compared to **NACV**. However the inverse is true for the second decay: **HST(BiO)** and **NACV** are within 2% of each other, while **LD** underestimates this decay by 9% as compared to **NACV**. As a result all three schemes give similar final S_2 populations, and even smaller differences are seen in the S_1 and S_0 populations throughout.

Despite differences in the electronic populations, the bond-dissociation reaction itself is found to be surprisingly consistent. For all schemes, between 97–99% of trajectories show the bond-dissociation during the simulation, with the average bond-breaking time ranging from 29.8–31.0 fs with standard deviation 4.0–7.4 fs (see Section S5.5 in the SI for more details). The ring-opening of butyrolactone is a very rapid, high energy reaction: exciting to S_2 requires 7.6 eV.[36] As a result differences in non-adiabatic coupling and resulting population decay are mostly irrelevant to the ballistic bond-breaking process itself. The TSH modeling of the reaction appears to require a qualitatively correct description only: the tested coupling approximations have a very small impact. The flawed **HST(CIV)** scheme delivers the correct reaction dynamics, although it varies significantly from the others after the bond-breaking process occurs around 30 fs and longer-time dynamics could show more significant differences. However **BA**, which shows differences in electronic populations throughout, also gives similar bond-dissociation dynamics.

As mentioned in the computational details, we have also tested the effect of phase correction methods on the TSH results. Butyrolactone is selected for analysis here, since the electronic populations are seemingly quite sensitive, showing the most variation between the different TSH schemes. Figure 8 shows the results for butyrolactone using **NACV** with different phase correction methods. Correcting the phase using the overlap between wavefunctions or using the scalar product of NAC vectors give almost identical results. However, using no phase correction at all gives entirely incorrect electronic populations: electronic decays are significantly underestimated. Clearly, a phase correction scheme is essential to TSH dynamics, and we recommend always running a test for this on any TSH dynamics run.

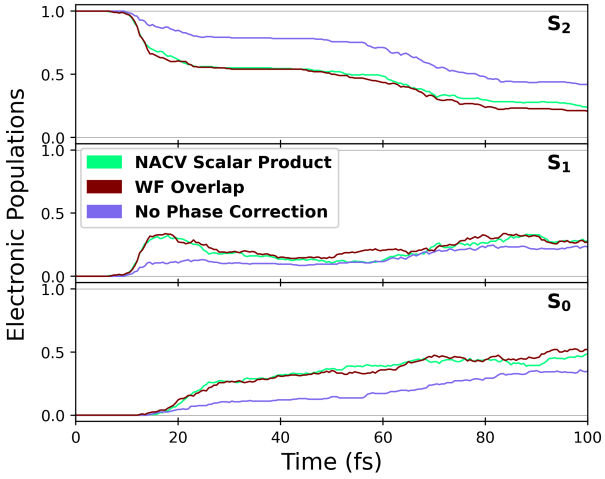

Figure 8: Electronic populations during the S_2 photoinduced ring-opening of butyrolactone (reaction **5**) using different phase correction methods.

For our final reaction we move to the ring-opening of furanone, a more gradual process, which occurs with a slower rate of dissociation previously described by a mono-exponential decay. Prior simulations have given a 140 fs time constant of dissociation, and prior experiment *ca.* 200 fs: this reaction thus provides a nice contrast to that of butyrolactone.[36] From Figure 7(b) we can see that the population decays are qualitatively similar for all schemes aside from **BA**. An overestimation of the early decay from the S_2 state again leads to differences from this scheme, with underestimated S_2 and overestimated S_0 populations throughout. In contrast to butyrolactone, the S_2 decay shows almost no variation between the other five schemes. Differences between populations are almost entirely contained to S_1 and S_0, and these variations are also minimal and less consistent than for the butyrolactone S_2 state. The main distinguishable feature is that the S_0 population given by **HST(CIV)** is noticeably lower throughout the simulation compared to the other schemes.

The fraction of C-O bonds dissociated throughout the simulations is also shown in Figure 7 for both butyrolactone (a) and furanone (b). In contrast to butyrolactone, where bond-dissociation takes place suddenly around 30 fs, the furanone bond dissociation is a slower process occurring over hundreds of femtoseconds, consistent with previous works.[36] For all schemes, dissociation starts around 30 fs, and apart from **BA** all schemes are very similar from this point onward. **HST(CIV)** describes the process reasonably, but slightly un-

derestimates the number of dissociated trajectories within the last 50 fs, by a small factor of ca. 7%. In contrast **BA** greatly underestimates the dissociation rate throughout, with 27% less trajectories undergoing bond dissociation within 150 fs. We see larger variation between schemes when describing the bond dissociation in furanone compared to butyrolactone, even though the electronic populations seem to show similar amounts of variation: differences in coupling schemes have a longer time to influence the dissociation process in the slower reaction.

5. DISCUSSION

Let us first briefly discuss some of the major issues which impact the accuracy of TSH in general. The failure to correctly account for decoherence, discussed in Section 2.1, is one of the most important issues and is usually handled by applying an adjustable ad-hoc correction.[43] This, along with the prediction of frustrated hops with insufficient kinetic energy, is what causes the mismatch between average "quantum probability" ($C_k C_k^*$) of each state and the fraction of actual trajectories in the state.[20,74] Another issue worth mentioning is the zero point energy (ZPE) leakage problem, which arises from the classical dynamics part: ZPE energy which should be "locked" in each normal mode can in fact transfer between modes, meaning reactions can occur below the quantum threshold of energy.[75] Issues also arise around CoIns, where NACVs change rapidly. Very local CoIns can even be missed and in such cases, a smaller dynamics timestep is necessary. Finally, in order to ensure energy conservation, the kinetic energy is scaled after hops to compensate for the sudden change in potential energy. The most adequate way is to rescale the velocity along the NACV.[70] However when the NACV is unknown, the scaling is usually done along the momentum or velocity directions, alternatives shown to be acceptable except for very large ensembles.[71] Despite these drawbacks and approximations inherent to TSH, this method often provides a good compromise between accuracy and cost and has been applied successfully to many photochemical problems.[22–24]

We can now discuss the difference in accuracy between the schemes tested here, within the scope of maximum TSH accuracy. Firstly, **HST(CIV)** is seen to give significantly different results to the other schemes in two cases: *trans*-AZB excitation and butyrolactone ring-opening. In the extreme case of *trans*-AZB, it even gives entirely unphysical results for the electronic populations. The rapid $S_1 \rightarrow S_0$ decay without large geometry change seen using **HST(CIV)** for this molecule is expected to have a large effect on the long-time dynamics beyond what is simulated here: since the *trans*-to-*cis* photoisomerization takes place on the S_1 state, deactivating this state entirely at early times will block this reaction from occurring. The failure of this scheme is linked to the approximation made to the coupling, which does not account for changes in orbital shapes or ordering. **HST(CIV)** is more likely to fail for "larger" systems with more orbitals within the CASSCF active space. However in some cases, such as butyrolactone, the reaction dynamics may be reasonably described even when electronic populations are inaccurate. As a result, it is challenging to predict and/or detect failure of **HST(CIV)** without a less-approximate reference. The specific failures of **HST(CIV)** are all resolved upon moving to the **HST(BiO)** scheme. The latter has almost identical computational cost when using CASSCF for electronic structure, thanks to a highly efficient bi-orthogonalisation procedure.

Secondly, **BA** gives different results to the other schemes for all reactions simulated here. For the best-cases, namely *cis*-AZM, *cis*-AZB and butyrolactone, differences are only seen in electronic populations with minimal impact on the reaction dynamics. However, for the *trans*-AZM and furanone cases these differences significantly impact the isomerization and dissociation processes themselves. For *trans*-AZB the unphysical $S_1 \rightarrow S_0$ decay is expected to cause entirely different longer-time dynamics as for **HST(CIV)**. In general **BA** overestimates decay rates far from CoIns, causing overestimated population decays in all reactions studied and failing to predict the delays before electronic population decays seen with all other schemes. We have also tested the effect of decreasing the timestep (Figure S26 in the SI), but this does not solve this **BA** issue. It was suggested in a different work,[29] which also proposed the **BA** scheme, that conditions be applied to **BA** such that decay is disallowed when the energy gap between states is larger than a threshold value. The application of this criterion to the **BA** scheme benchmarked in this work could significantly improve results using this scheme. This coupling overestimation likely also causes the second main issue seen using **BA**, i.e., a significantly higher proportion of backhops, especially for the smallest systems. However, despite these issues **BA** still shows promise as a scheme which can be used when neither NACV or overlaps are possible. Unlike **HST(CIV)**, the failures with **BA** are systematic, which makes improvements to this scheme simple to determine.

Finally, it has been seen throughout that, excluding these two more approximate schemes (**HST(CIV)** and **BA**), the other three TSH schemes tested in this study give remarkably similar results, not only qualitatively in their correct description of reaction dynamics, but quantitatively also. On comparing electronic populations and either isomer fractions or bond-dissociation events, only minor differences are seen between **LD**, **HST(BiO)**, and **NACV** despite the different approximations employed in the TSH methodology. Only for the *cis*-AZM and the butyrolactone are non-negligible differences seen between any of these three schemes. For *cis*-AZM, **LD** gives around 10% more $S_1 \rightarrow S_0$ decay within 145 fs compared to **NACV** and **HST(BiO)**. In the literature, it has been suggested that **LD** may give better results at regions of highly localized non-adiabatic coupling, as it correctly captures the coupling with standard time-steps while **NACV** can require much shorter time-steps to be fully converged.[76] However, upon testing the convergence with time-step size for this reaction, we do not find that decreasing the time-step in **NACV** dynamics increases the overall amount of population which decays over the reaction (see Figure S25 of the SI). That is to say, more coupling is not captured using smaller time-steps, and thus the differences in this case cannot be explained by a failure to converge the **NACV** results. For butyrolactone, the three schemes vary by around 10% in S_2 decay throughout. However, for both these reactions, the

differences are less visible in the reaction dynamics process itself. For *cis*-AZM, while at certain times the **LD** fraction is different, there are no clear differences which persist throughout the simulations. For butyrolactone the photo-dissociation around 30 fs is almost identical despite different S_2 populations at this point. Overall, electronic populations tend to be more sensitive to the TSH scheme used, in comparison to the isomeric fractions and/or dissociation times.

Both **HST(BiO)** and **LD** present significant computational saving over **NACV** (when utilizing the efficient biorthonormalisation procedure), without compromising on accuracy, being at least 2 times (and in the large AZB case, nearly 10 times) faster to run (Table S8 in the SI). Both these schemes have been demonstrated within this study to be excellent alternatives to **NACV** TSH simulations. **HST(BiO)** can be run within a single program (OpenMOLCAS[37]), simplifying use, while both the SHARC[65] and Newton-X[68] implementations of **LD** have more options for expert users to tune dynamics simulations.

6. CONCLUSIONS

In this work, we have benchmarked the impact of different commonly used approximations to the coupling term, made within five schemes based on the popular trajectory surface hopping method. The coupling term determines the location of hops between the electronic states, and thus could have a large influence on simulation results. Both the electronic populations and the photoreaction dynamics have been studied on a representative series of photoreactions, to analyze the impact of these approximations.

In general, the electronic populations are more sensitive to differences between surface hopping schemes, while the overall reaction dynamics seen in, e.g., quantum yields and rates of bond dissociation, is much more resilient to the scheme used. For example, the *cis*-AZM molecule shows a range of 10% in the electronic decays between schemes, but no consistent difference in fractions of isomers and very similar estimated quantum yields of isomerization. Another example is the butyrolactone ring-opening, where clear differences in the S_2 populations do not lead to different mean dissociation times, which vary by only 0.4 fs. While the electronic populations can be sensitive to the approximations made within TSH, the photoreactions themselves are clearly much less influenced. The exceptions to this rule are seen when using **BA**: the *trans*-AZM photoisomerization process and the furanone bond-dissociation are significantly impacted by early overestimation of non-adiabatic decay. In general, unless one of the most approximate schemes is used (**BA** or **HST(CIV)**), care towards approximations used within TSH is more critical when attempting to extract quantitative information about photoreactions, or when accurate descriptions of population decays are required, such as when attempting to model spectroscopies which track electronic decays.

HST(CIV) is clearly seen to be one of the worse schemes tested and should be avoided. In at least one case (*trans*-AZB), it gives entirely unphysical simulations. Even though this scheme can give similar results for photoreaction dynamics even when electronic populations are noticeably different from the other schemes (e.g. for *cis*-AZB), it is impossible without further simulations or experimental data to know if estimated electronic decays and/or reaction dynamics are physical or not. **HST(BiO)** on the other hand is seen to well reproduce the **NACV** dynamics in all reactions at an affordable cost. Thanks to the highly efficient bio-orthogonalisation procedure available for CASSCF wavefunctions, moving from **HST(CIV)** to **HST(BiO)** adds almost no additional computational cost, and we therefore recommend the systematic use of **HST(BiO)** over **HST(CIV)**. While **HST(CIV)** was previously the only default (and only) TSH scheme available in OpenMOLCAS,[37] **HST(BiO)** has been implemented in OpenMOLCAS as part of this work, and is now the default way to run TSH within this code.

The **BA** scheme is also seen to be flawed, giving similar unphysical results for the *trans*-AZB case and overestimating coupling far from CoIns in every reaction tested. For furanone and *trans*-AZM, this scheme inaccurately describes not just the electronic populations but also the overall reaction dynamics. However, unlike **HST(CIV)** where failure is unpredictable, **BA** systematically overestimates the coupling far from CoIns.

Finally, **LD** matches very well the results of **NACV** and **HST(BiO)** simulations in all cases except the *cis*-AZM. In this case, the electronic populations vary by around 10%. Decreasing the timestep for the **NACV** scheme for this reaction simulation has no impact on the **NACV** results: the differences do not seem to be caused by insufficient convergence of the **NACV** results with timestep length. We do however highlight that the overall reaction dynamics in this case is hardly affected.

The overall simulation results for the reactions studied are very similar with all schemes beside **HST(CIV)** and **BA**, which both lead to incorrect dynamics for certain cases. These schemes could still be used for exploratory dynamics as previously suggested.[29] Both **LD** and **HST(BiO)** have a similar computational cost, which is significantly lower than **NACV**. This is due to the use of the wavefunction overlap matrix to approximate the coupling (in two different ways), avoiding the bottleneck of calculating the non-adiabatic coupling vectors. These two schemes are demonstrated to be excellent alternatives to **NACV** surface hopping, with the approximations made within the methodologies having little effect on the overall statistical average of the ensembles.

ACKNOWLEDGEMENTS

The authors would like to thank Mario Barbatti for kindly providing template files for the development of Newton-X interfaces, Alessio Valentini for helpful discussion on the nature of the surface hopping code within OpenMOLCAS, and Sebastian Mai for insights into the local diabatization scheme and assistance in fixing implementation issues. We would also like to thank one of the anonymous reviewers for bringing to our attention the **BA** scheme. This work was performed using HPC resources from GENCI-IDRIS (Grant 2021-101353) and CCIPL/Glicid (*Le centre de calcul intensif des Pays de la Loire*). I.M. acknowledges thesis funding from Nantes University.

SUPPORTING INFORMATION AVAILABLE

Full derivations for TSH equations and description of the FSSH algorithm. Full description of the **LD** scheme. Active spaces. Proof of convergence with number of trajectories. Additional analysis for reactions studied. *Cis* and *Trans*-AZM: analysis of hop locations. *Trans*-AZB: fractions of isomers for both active spaces, magnified sections of population graphs, time-coupling graphs, example of change in orbital character between timesteps under the **HST(CIV)** scheme, test of decreasing timestep size using **HST(CIV)**, comparison of average PES with both active spaces for **NACV**. *Cis*-AZB: analysis of hop locations, reduced active space population graphs and isomer fractions. Butyrolactone: bond-dissociation details, electronic populations using LD with/without substeps and with two ways to calculate hopping probabilities, test of decreasing number of substeps with the **NACV** scheme. Description of phase correction schemes and effects on the electronic populations of *trans*-AZM and butyrolactone.

REFERENCES

(1) Barber, J. Photochemistry: A Quantum Step towards Artificial Photosynthesis. *Nature* **1984**, *307*, 596–596.

(2) Mura, S.; Nicolas, J.; Couvreur, P. Stimuli-Responsive Nanocarriers for Drug Delivery. *Nat. Mater.* **2013**, *12*, 991–1003.

(3) Li, L.; Shemetov, A. A.; Baloban, M.; Hu, P.; Zhu, L.; Shcherbakova, D. M.; Zhang, R.; Shi, J.; Yao, J.; Wang, L. V.; Verkhusha, V. V. Small Near-Infrared Photochromic Protein for Photoacoustic Multi-Contrast Imaging and Detection of Protein Interactions in Vivo. *Nat. Commun.* **2018**, *9*, 2734.

(4) Klajn, R. Spiropyran-Based Dynamic Materials. *Chem. Soc. Rev.* **2014**, *43*, 148–184.

(5) Ru, Y.; Shi, Z.; Zhang, J.; Wang, J.; Chen, B.; Huang, R.; Liu, G.; Yu, T. Recent Progress of Photochromic Materials towards Photocontrollable Devices. *Mater. Chem. Front.* **2021**, *5*, 7737–7758.

(6) Leydecker, T.; Herder, M.; Pavlica, E.; Bratina, G.; Hecht, S.; Orgiu, E.; Samorì, P. Flexible Non-Volatile Optical Memory Thin-Film Transistor Device with over 256 Distinct Levels Based on an Organic Bicomponent Blend. *Nat. Nanotechnol.* **2016**, *11*, 769–775.

(7) Evans, R. C., Douglas, P., Burrow, H. D., Eds. *Applied Photochemistry*; Springer Netherlands: Dordrecht, 2013.

(8) Ikeda, T.; Tsutsumi, O. Optical Switching and Image Storage by Means of Azobenzene Liquid-Crystal Films. *Science* **1995**, *268*, 1873–1875.

(9) Velema, W. A.; Szymanski, W.; Feringa, B. L. Photopharmacology: Beyond Proof of Principle. *J. Am. Chem. Soc.* **2014**, *136*, 2178–2191.

(10) Hou, L.; Zhang, X.; Pijper, T. C.; Browne, W. R.; Feringa, B. L. Reversible Photochemical Control of Singlet Oxygen Generation Using Diarylethene Photochromic Switches. *J. Am. Chem. Soc.* **2014**, *136*, 910–913.

(11) Sousa, S. F.; Souza, B. L.; Barros, C. L.; Patrocinio, A. O. T. Inorganic Photochemistry and Solar Energy Harvesting: Current Developments and Challenges to Solar Fuel Production. *Int. J. Photoenergy* **2019**, *2019*, 1–23.

(12) Balzani, V.; Credi, A.; Venturi, M. Photochemical Conversion of Solar Energy. *ChemSusChem* **2008**, *1*, 26–58.

(13) Parida, B.; Iniyan, S.; Goic, R. A Review of Solar Photovoltaic Technologies. *Renewable Sustainable Energy Rev.* **2011**, *15*, 1625–1636.

(14) Cambié, D.; Dobbelaar, J.; Riente, P.; Vanderspikken, J.; Shen, C.; Seeberger, P. H.; Gilmore, K.; Debije, M. G.; Noël, T. Energy-Efficient Solar Photochemistry with Luminescent Solar Concentrator Based Photomicroreactors. *Angew. Chem., Int. Ed.* **2019**, *58*, 14374–14378.

(15) Anastas, P.; Eghbali, N. Green Chemistry: Principles and Practice. *Chem. Soc. Rev.* **2010**, *39*, 301–312.

(16) Oelgemöller, M. Solar Photochemical Synthesis: From the Beginnings of Organic Photochemistry to the Solar Manufacturing of Commodity Chemicals. *Chem. Rev.* **2016**, *116*, 9664–9682.

(17) Lasorne, B.; Worth, G. A.; Robb, M. A. Excited-State Dynamics. *Wiley Interdiscip. Rev.: Comput. Mol. Sci.* **2011**, *1*, 460–475.

(18) Förster, T. Diabatic and Adiabatic Processes in Photochemistry. *Pure Appl. Chem.* **1970**, *24*, 443–450.

(19) Tully, J. C.; Preston, R. K. Trajectory Surface Hopping Approach to Nonadiabatic Molecular Collisions: The Reaction of H^+ with D_2. *J. Chem. Phys.* **1971**, *55*, 562–572.

(20) Barbatti, M. Nonadiabatic Dynamics with Trajectory Surface Hopping Method. *Wiley Interdiscip. Rev.: Comput. Mol. Sci.* **2011**, *1*, 620–633.

(21) Tully, J. C. Molecular Dynamics with Electronic Transitions. *J. Chem. Phys.* **1990**, *93*, 1061–1071.

(22) Yu, J. K.; Bannwarth, C.; Liang, R.; Hohenstein, E. G.; Martínez, T. J. Nonadiabatic Dynamics Simulation of the Wavelength-Dependent Photochemistry of Azobenzene Excited to the $n\pi^*$ and $\pi\pi^*$ Excited States. *J. Am. Chem. Soc.* **2020**, *142*, 20680–20690.

(23) Sellner, B.; Ruckenbauer, M.; Stambolić, I.; Barbatti, M.; Aquino, A. J. A.; Lischka, H. Photodynamics of Azomethane: A Nonadiabatic Surface-Hopping Study. *J. Phys. Chem. A* **2010**, *114*, 8778–8785.

(24) Pathak, S.; Ibele, L. M.; Boll, R.; Callegari, C.; Demidovich, A.; Erk, B.; Feifel, R.; Forbes, R.; Di Fraia, M.; Giannessi, L.; Hansen, C. S.; Holland, D. M. P.; Ingle, R. A.; Mason, R.; Plekan, O.; Prince, K. C.; Rouzée, A.; Squibb, R. J.; Tross, J.; Ashfold, M. N. R.; Curchod, B. F. E.; Rolles, D. Tracking the Ultraviolet-Induced Photochemistry of Thiophenone during and after Ultrafast Ring Opening. *Nat. Chem.* **2020**, *12*, 795–800.

(25) Granucci, G.; Persico, M.; Toniolo, A. Direct Semiclassical Simulation of Photochemical Processes with Semiempirical Wave Functions. *J. Chem. Phys.* **2001**, *114*, 10608–10615.

(26) Hammes-Schiffer, S.; Tully, J. C. Proton Transfer in Solution: Molecular Dynamics with Quantum Transitions. *J. Chem. Phys.* **1994**, *101*, 4657–4667.
(27) Shu, Y.; Zhang, L.; Chen, X.; Sun, S.; Huang, Y.; Truhlar, D. G. Nonadiabatic Dynamics Algorithms with Only Potential Energies and Gradients: Curvature-Driven Coherent Switching with Decay of Mixing and Curvature-Driven Trajectory Surface Hopping. *J. Chem. Theory Comput.* **2022**, *18*, 1320–1328.
(28) Fabiano, E.; Keal, T.; Thiel, W. Implementation of Surface Hopping Molecular Dynamics Using Semiempirical Methods. *Chem. Phys.* **2008**, *349*, 334–347.
(29) T. do Casal, M.; Toldo, J. M.; Pinheiro Jr, M.; Barbatti, M. Fewest Switches Surface Hopping with Baeck-An Couplings. *Open Res Europe* **2022**, *1*, 49.
(30) Nangia, S.; Jasper, A. W.; Miller, T. F.; Truhlar, D. G. Army Ants Algorithm for Rare Event Sampling of Delocalized Nonadiabatic Transitions by Trajectory Surface Hopping and the Estimation of Sampling Errors by the Bootstrap Method. *The Journal of Chemical Physics* **2004**, *120*, 3586–3597.
(31) Oloyede, P.; Mil'nikov, G.; Nakamura, H. Generalized Trajectory Surface Hopping Method Based on the Zhu-Nakamura Theory. *The Journal of Chemical Physics* **2006**, *124*, 144110.
(32) Ruckenbauer, M.; Barbatti, M.; Sellner, B.; Muller, T.; Lischka, H. Azomethane: Nonadiabatic Photodynamical Simulations in Solution. *J. Phys. Chem. A* **2010**, *114*, 12585–12590.
(33) Quick, M.; Dobryakov, A. L.; Gerecke, M.; Richter, C.; Berndt, F.; Ioffe, I. N.; Granovsky, A. A.; Mahrwald, R.; Ernsting, N. P.; Kovalenko, S. A. Photoisomerization Dynamics and Pathways of Trans- and Cis-Azobenzene in Solution from Broadband Femtosecond Spectroscopies and Calculations. *J. Phys. Chem. B* **2014**, *118*, 8756–8771.
(34) Satzger, H.; Spörlein, S.; Root, C.; Wachtveitl, J.; Zinth, W.; Gilch, P. Fluorescence Spectra of Trans- and Cis-Azobenzene – Emission from the Franck–Condon State. *Chem. Phys. Lett.* **2003**, *372*, 216–223.
(35) Tan, E. M. M.; Amirjalayer, S.; Smolarek, S.; Vdovin, A.; Zerbetto, F.; Buma, W. J. Fast Photodynamics of Azobenzene Probed by Scanning Excited-State Potential Energy Surfaces Using Slow Spectroscopy. *Nat. Commun.* **2015**, *6*, 5860.
(36) Schalk, O.; Galiana, J.; Geng, T.; Larsson, T. L.; Thomas, R. D.; Fdez. Galván, I.; Hansson, T.; Vacher, M. Competition between Ring-Puckering and Ring-Opening Excited State Reactions Exemplified on 5H-furan-2-one and Derivatives. *J. Chem. Phys.* **2020**, *152*, 064301.
(37) Fdez. Galván, I.; Vacher, M.; Alavi, A.; Angeli, C.; Aquilante, F.; Autschbach, J.; Bao, J. J.; Bokarev, S. I.; Bogdanov, N. A.; Carlson, R. K.; Chibotaru, L. F.; Creutzberg, J.; Dattani, N.; Delcey, M. G.; Dong, S. S.; Dreuw, A.; Freitag, L.; Frutos, L. M.; Gagliardi, L.; Gendron, F.; Giussani, A.; González, L.; Grell, G.; Guo, M.; Hoyer, C. E.; Johansson, M.; Keller, S.; Knecht, S.; Kovačević, G.; Källman, E.; Li Manni, G.; Lundberg, M.; Ma, Y.; Mai, S.; Malhado, J. P.; Malmqvist, P. Å.; Marquetand, P.; Mewes, S. A.; Norell, J.; Olivucci, M.; Oppel, M.; Phung, Q. M.; Pierloot, K.; Plasser, F.; Reiher, M.; Sand, A. M.; Schapiro, I.; Sharma, P.; Stein, C. J.; Sørensen, L. K.; Truhlar, D. G.; Ugandi, M.; Ungur, L.; Valentini, A.; Vancoillie, S.; Veryazov, V.; Weser, O.; Wesołowski, T. A.; Widmark, P.-O.; Wouters, S.; Zech, A.; Zobel, J. P.; Lindh, R. OpenMolcas: From Source Code to Insight. *J. Chem. Theory Comput.* **2019**, *15*, 5925–5964.
(38) Barbatti, M.; Ruckenbauer, M.; Plasser, F.; Pittner, J.; Granucci, G.; Persico, M.; Lischka, H. Newton-X: A Surface-Hopping Program for Nonadiabatic Molecular Dynamics. *Wiley Interdiscip. Rev.: Comput. Mol. Sci.* **2014**, *4*, 26–33.
(39) Hayashi, S.; Tajkhorshid, E.; Schulten, K. Photochemical Reaction Dynamics of the Primary Event of Vision Studied by Means of a Hybrid Molecular Simulation. *Biophys. J.* **2009**, *96*, 403–416.
(40) Fermanian Kammerer, C.; Lasser, C. Single Switch Surface Hopping for Molecular Dynamics with Transitions. *J. Chem. Phys.* **2008**, *128*, 144102.
(41) Lasser, C.; Swart, T. Single Switch Surface Hopping for a Model of Pyrazine. *J. Chem. Phys.* **2008**, *129*, 034302.
(42) Blais, N. C.; Truhlar, D. G. Trajectory-surface-hopping study of Na(3p 2P) + H2 → Na(3s 2S) + H2(v',j',θ'. *J. Chem. Phys.* **1983**, *79*, 1334–1342.
(43) Granucci, G.; Persico, M. Critical Appraisal of the Fewest Switches Algorithm for Surface Hopping. *J. Chem. Phys.* **2007**, *126*, 134114.
(44) Zhu, C.; Jasper, A. W.; Truhlar, D. G. Non-Born-Oppenheimer Liouville-von Neumann Dynamics. Evolution of a Subsystem Controlled by Linear and Population-Driven Decay of Mixing with Decoherent and Coherent Switching. *Journal of Chemical Theory and Computation* **2005**, *1*, 527–540.
(45) Jasper, A. W.; Stechmann, S. N.; Truhlar, D. G. Fewest-switches with time uncertainty: A modified trajectory surface-hopping algorithm with better accuracy for classically forbidden electronic transitions. *The Journal of Chemical Physics* **2002**, *116*, 5424–5431.
(46) Müller, U.; Stock, G. Surface-hopping modeling of photoinduced relaxation dynamics on coupled potential-energy surfaces. *The Journal of Chemical Physics* **1997**, *107*, 6230–6245.
(47) Pittner, J.; Lischka, H.; Barbatti, M. Optimization of Mixed Quantum-Classical Dynamics: Time-derivative Coupling Terms and Selected Couplings. *Chem. Phys.* **2009**, *356*, 147–152.
(48) Plasser, F.; Ruckenbauer, M.; Mai, S.; Oppel, M.; Marquetand, P.; González, L. Efficient and Flexible Computation of Many-Electron Wave Function Overlaps. *J. Chem. Theory Comput.* **2016**, *12*, 1207–1219.
(49) Tran, L. N.; Shea, J. A. R.; Neuscamman, E. Tracking Excited States in Wave Function Optimization Using Density Matrices and Variational Principles. *J. Chem. Theory Comput.* **2019**, *15*, 4790–4803.

(50) Martínez, T. J. Ab Initio Molecular Dynamics around a Conical Intersection: Li(2p) + H2. *Chem. Phys. Lett.* **1997**, *272*, 139–147.
(51) Groenhof, G.; Bouxin-Cademartory, M.; Hess, B.; de Visser, S. P.; Berendsen, H. J. C.; Olivucci, M.; Mark, A. E.; Robb, M. A. Photoactivation of the Photoactive Yellow Protein: Why Photon Absorption Triggers a Trans-to-Cis Isomerization of the Chromophore in the Protein. *J. Am. Chem. Soc.* **2004**, *126*, 4228–4233.
(52) Groenhof, G.; Schäfer, L. V.; Boggio-Pasqua, M.; Goette, M.; Grubmüller, H.; Robb, M. A. Ultrafast Deactivation of an Excited Cytosine-Guanine Base Pair in DNA. *J. Am. Chem. Soc.* **2007**, *129*, 6812–6819.
(53) Malmqvist, P. A. Calculation of Transition Density Matrices by Nonunitary Orbital Transformations. *Int. J. Quantum Chem.* **1986**, *30*, 479–494.
(54) Nakamura, H.; Truhlar, D. G. The direct calculation of diabatic states based on configurational uniformity. *The Journal of Chemical Physics* **2001**, *115*, 10353–10372.
(55) Nakamura, H.; Truhlar, D. G. Direct diabatization of electronic states by the fourfold way. II. Dynamical correlation and rearrangement processes. *The Journal of Chemical Physics* **2002**, *117*, 5576–5593.
(56) Yang, K. R.; Xu, X.; Truhlar, D. G. Direct diabatization of electronic states by the fourfold-way: Including dynamical correlation by multi-configuration quasidegenerate perturbation theory with complete active space self-consistent-field diabatic molecular orbitals. *Chemical Physics Letters* **2013**, *573*, 84–89.
(57) Baeck, K. K.; An, H. Practical approximation of the non-adiabatic coupling terms for same-symmetry interstate crossings by using adiabatic potential energies only. *The Journal of Chemical Physics* **2017**, *146*, 064107.
(58) Yao, K.; Herr, J. E.; Toth, D. W.; Mckintyre, R.; Parkhill, J. The TensorMol-0.1 Model Chemistry: A Neural Network Augmented with Long-Range Physics. *Chem. Sci.* **2018**, *9*, 2261–2269.
(59) Chandrasekaran, A.; Kamal, D.; Batra, R.; Kim, C.; Chen, L.; Ramprasad, R. Solving the Electronic Structure Problem with Machine Learning. *npj Comput. Mater.* **2019**, *5*, 22.
(60) Roos, B. O.; Taylor, P. R.; Sigbahn, P. E. A Complete Active Space SCF Method (CASSCF) Using a Density Matrix Formulated Super-CI Approach. *Chem. Phys.* **1980**, *48*, 157–173.
(61) Roos, B. O.; Lindh, R.; Malmqvist, P.-Å.; Veryazov, V.; Widmark, P.-O. Main Group Atoms and Dimers Studied with a New Relativistic ANO Basis Set. *J. Phys. Chem. A* **2004**, *108*, 2851–2858.
(62) Hehre, W. J.; Ditchfield, R.; Pople, J. A. Self—Consistent Molecular Orbital Methods. XII. Further Extensions of Gaussian—Type Basis Sets for Use in Molecular Orbital Studies of Organic Molecules. *J. Chem. Phys.* **1972**, *56*, 2257–2261.
(63) Hariharan, P. C.; Pople, J. A. The Influence of Polarization Functions on Molecular Orbital Hydrogenation Energies. *Theoret. Chim. Acta* **1973**, *28*, 213–222.
(64) Aquilante, F.; Lindh, R.; Bondo Pedersen, T. Unbiased Auxiliary Basis Sets for Accurate Two-Electron Integral Approximations. *J. Chem. Phys.* **2007**, *127*, 114107.
(65) Mai, S.; Richter, M.; Heindl, M.; Menger, M. F. S. J.; Atkins, A.; Ruckenbauer, M.; Plasser, F.; Ibele, L. M.; Kropf, S.; Oppel, M.; Marquetand, P.; González, L. SHARC2.1: Surface Hopping Including Arbitrary Couplings — Program Package for Non-Adiabatic Dynamics. sharc-md.org, 2019.
(66) Richter, M.; Marquetand, P.; González-Vázquez, J.; Sola, I.; González, L. SHARC: Ab Initio Molecular Dynamics with Surface Hopping in the Adiabatic Representation Including Arbitrary Couplings. *J. Chem. Theory Comput.* **2011**, *7*, 1253–1258.
(67) Mai, S.; Marquetand, P.; González, L. Nonadiabatic Dynamics: The SHARC Approach. *Wiley Interdiscip. Rev.: Comput. Mol. Sci.* **2018**, *8*, e1370.
(68) Barbatti, M.; Granucci, G.; Ruckenbauer, M.; Plasser, F.; Crespo-Otero, R.; Pittner, J.; Persico, M.; Lischka, H. NEWTON-X: A package for Newtonian Dynamics Close to the Crossing Seam (v. 2.2). Available via the Internet at www.newtonx.org, 2018.
(69) Shu, Y.; Zhang, L.; Truhlar, D. G. Surface Hopping with Arbitrary Couplings - MN extension. https://comp.chem.umn.edu/sharc-mn, 2022.
(70) Herman, M. F. Nonadiabatic semiclassical scattering. I. Analysis of generalized surface hopping procedures. *The Journal of Chemical Physics* **1984**, *81*, 754–763.
(71) Barbatti, M. Velocity Adjustment in Surface Hopping: Ethylene as a Case Study of the Maximum Error Caused by Direction Choice. *Journal of Chemical Theory and Computation* **2021**, *17*, 3010–3018.
(72) Ciminelli, C.; Granucci, G.; Persico, M. The Photoisomerization Mechanism of Azobenzene: A Semiclassical Simulation of Nonadiabatic Dynamics. *Chem. Eur. J.* **2004**, *10*, 2327–2341.
(73) Pederzoli, M.; Pittner, J.; Barbatti, M.; Lischka, H. Nonadiabatic Molecular Dynamics Study of the Cis - Trans Photoisomerization of Azobenzene Excited to the S_1 State. *J. Phys. Chem. A* **2011**, *115*, 11136–11143.
(74) Subotnik, J. E.; Jain, A.; Landry, B.; Petit, A.; Ouyang, W.; Bellonzi, N. Understanding the Surface Hopping View of Electronic Transitions and Decoherence. *Annu. Rev. Phys. Chem.* **2016**, *67*, 387–417.
(75) Mukherjee, S.; Barbatti, M. A Hessian-Free Method to Prevent Zero-Point Energy Leakage in Classical Trajectories. *Journal of Chemical Theory and Computation* **2022**, *18*, 4109–4116.
(76) Plasser, F.; Granucci, G.; Pittner, J.; Barbatti, M.; Persico, M.; Lischka, H. Surface Hopping Dynamics Using a Locally Diabatic Formalism: Charge Transfer in the Ethylene Dimer Cation and Excited State Dynamics in the 2-Pyridone Dimer. *J. Chem. Phys.* **2012**, *137*, 22A514.

Graphical TOC Entry